PERGAMON

International Journal of Solids and Structures 38 (2001) 75–90

INTERNATIONAL JOURNAL OF SOLIDS and STRUCTURES

www.elsevier.com/locate/ijsolstr

Boundary element analysis of cracked film–substrate media

Yen-Ling Chung *, Chin-Foung Pon

Department of Construction Engineering, National Taiwan University of Science and Technology, Taipei, Taiwan, ROC

Received 29 March 1999; in revised form 14 September 1999

Abstract

This study evaluates the stress behavior of a cracked film–substrate medium by applying the multi-region boundary element method. Four problems addressed herein are the crack tip within a film, the crack tip terminating at the interface, interface debonding, and the crack penetrating into the substrate. The multi-region boundary element method is initially developed and, then, the stress intensity factors or the energy release rates are evaluated according to the different stress singularities of the four considered problems. These results indicate that the stress intensity factors or the energy release rates of the four problems rely not only on the different elastic mismatches and crack lengths, but also on the thickness ratio of the film and the substrate.

Keywords: Multi-region boundary element method; Cracked film–substrate medium; Energy release rate; Stress intensity factor

1. Introduction

Owing to the high performance demands of engineering devices, coating technology profoundly enhances the lifetime of materials. In coating processes, the thermal stress exists due to the difference among the thermal expansion coefficients of the coating and the substrate. Consequently, the film–substrate composite medium may incur cracking or debonding. The cracking path or the debonding pattern is related not only to the residual thermal stress, but also to the relative toughness (Kral et al., 1996) or relative melting temperature of the film–substrate medium (Suo and Hutchinson, 1989; Thornton, 1989). However, cracking may originate from the edge of the film and extend along the direction perpendicular to the interfaces (Fig. 1(a)); cracking may stop at the interface (Fig. 1(b)). When the crack tip reaches the interface of the film–substrate medium, the crack may bifurcate onto the interface (Fig. 1(c)) if the interface has a decreased strength; the crack may also penetrate into the substrate if the toughness of the substrate is low (Fig. 1(d)). Although the cracking patterns have received considerable attention, the stress behaviors all of the crack patterns must be fully realized. Therefore, this study evaluates the stress behaviors of the four problems illustrated in Fig. 1.

Problems associated with the cracked film–substrate structure have been studied (Cook and Erdogan, 1972; Gecit, 1979; Lu and Erdogan, 1983a,b; Chen, 1984). Cook and Erdogan (1972) analyzed the problem

* Corresponding author. Tel.: +886-2-2737-6558.
E-mail address: chung@hp.ct.ntust.edu.tw (Y.-L. Chung).

0020-7683/00/$ - see front matter
PII: S0020-7683(00)00008-1

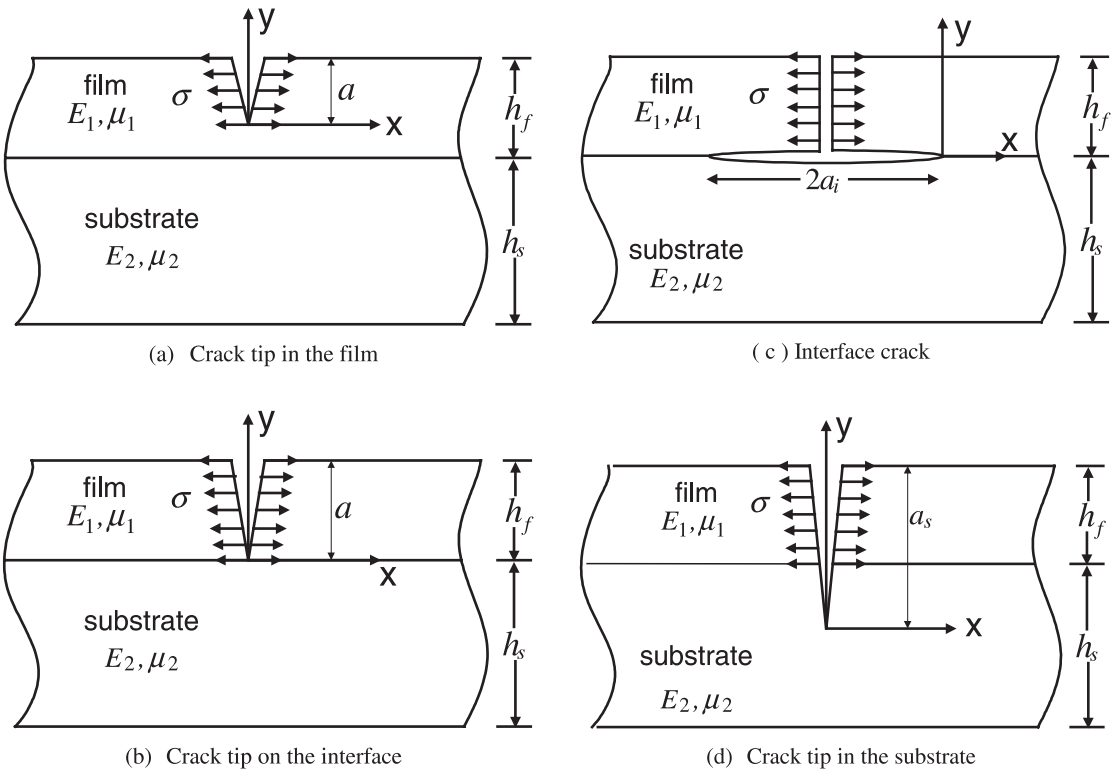

Fig. 1. The geometry of the cracked film–substrate medium: (a) crack tip inside the film; (b) crack tip on the interface; (c) crack along the interface; and (d) crack tip inside the substrate.

of two elastic bonded half planes containing a crack perpendicular to the interface. According to their results, the power of stress singularity at the crack tip of the interface is not −1/2. Moreover, Gecit (1979) investigated the plane problem of a cracked elastic surface layer bonded to an elastic half space, indicating that if the length of the edge crack is short, the stress behavior at the crack tip is proportional to $r^{-1/2}$. However, if the crack tip is near the interface, the power of stress singularity is 0.8248 for aluminum–epoxy medium and 0.6205 for steel–aluminum bonded material. Related investigations (Lu and Erdogan, 1983a,b; Chen, 1984) obtained similar results for the crack normal to and terminating at a bi-material interface, the stress field is proportional to r^{-s}, where s denotes the stress singularity exponent and is related to Dundurs' parameters α and β. However, most analytical results have mainly focused on the power of stress singularities at the crack tips (Cook and Erdogan, 1972; Gecit, 1979; Lu and Erdogan, 1983a,b; Chen, 1984); the numerical results are limited to a few unique cases. Beuth (1992) presented solutions for problems involving the crack tip within a film and crack tip on the interface over the full range of practical elastic mismatches, when applying the finite element method.

One of important failure modes for film–substrate systems is that the crack penetrates the full range of the film and bifurcates onto the interface (Fig. 1(c)). The well-known displacement and stress oscillations arise around the tips of an interface crack (Willams, 1959; England, 1965; Erdogan, 1988; Rice, 1988). To evaluate the oscillatory stress intensity factor (SIF) of interface cracks, the auxiliary field is taken as the singular crack tip field for an interfacial crack (Matos et al., 1989). However, calculating the energy release rate (ERR) or the overall SIF does not encounter oscillation problems (Ye et al., 1992; Tan and Gao, 1990).

Ye et al. (1992) provided the approximate formulas of the dimensionless ERR for the interface crack of the film–substrate medium by the finite element calculation.

If the toughness of a substrate is sufficiently low, the crack penetrates into the substrate (Fig. 1(d)). While addressing this problem, Beuth (1992) evaluated the approximate formula of the dimensionless ERR and Ye et al. (1992) examined the critical film thickness to avert cracking. According to Beuth (1992), the dimensionless ERR rapidly decays when the crack tip is near the interface. In addition, the dimensionless ERR approaches a constant value when the crack tip is somewhat farther from the interface. A related problem of Fig. 1(d) is a crack kinking out of an interface crack (He and Hutchinson, 1989; Akisanya and Fleck, 1994). He and Hutchinson (1989) derived the theory of kinking of an interface, that provides the SIF and ERR of the kinked crack in terms of the corresponding quantities for the interface crack prior to kinking. Akisanya and Fleck (1994) discussed the role of the T-stresses and the interfacial phase angle in influencing the selection of crack path.

Most investigations assumed that the thin film is bonded to a dissimilar semi-infinite substrate material (Gecit, 1979; Chen, 1984; Beuth, 1992; Ye et al., 1992), whereas the effects of the thickness ratio of the film and substrate have seldom been considered. However, according to Lu and Erdogan (1983a), the SIF of the problem of Fig. 1(d) is related to the thickness ratio of the film–substrate system. Therefore, although previous literature offers solutions to problems resembling those addressed herein, this study emphasizes not only the material properties and the crack length, but also the thickness ratio of the film and the substrate. Moreover, results in this study provide further insight into the stress behavior of the film–substrate composite materials.

This study also addresses the problem of compressive stress acting on the surfaces of the crack in the film–substrate body of a finite dimension. The SIF or ERR is examined at the crack tip while considering different crack lengths, different material combinations, and different thickness ratios of the film and the substrate. As generally known, analytical solutions can be obtained only for simple geometry or infinite body. In addition, the boundary element method (BEM) aptly resolves the problem involving stress concentration. Therefore, this study also develops the multi-region boundary element method and applies it to evaluate the cracked film–substrate medium. Also adopted herein is the numerical solution of the finite element method of Beuth (1992) and Ye et al. (1992), which is used to compare with the solution in this study. In all the cases found in Fig. 1, the SIF or the ERR obtained from the current multi-region BEM correlates well with those studied in Beuth (1992) and Ye et al. (1992) for the nearly infinite substrate.

2. Multi-region boundary element method

2.1. Boundary element method

For homogeneous and isotropic elastic bodies, the boundary integral equation neglecting the body force is written in the following form (Becker, 1992):

$$C_{ij}(P)u_i(P) = \int_s t_i(Q)U_{ij}(P,Q)\,\mathrm{d}(S)_Q - \int_s u_i(Q)T_{ij}(P,Q)\,\mathrm{d}(S)_Q, \tag{1}$$

where the kernel functions U_{ij} and T_{ij} denote the fundamental displacement and traction, respectively, and u_i and t_i represent the displacement and traction vectors on the boundary S. The value of the coefficient $C_{ij}(P)$ depending on the boundary conditions can be estimated by applying the technique of rigid body translation.

The boundary S can be discretized into many elements for numerical calculation. When the isoparametric quadratic elements in local coordinates of $0 \leqslant \xi \leqslant 1$ are used, Eq. (1) can be rewritten as

$$C_{ij}(P)u_i(P) = \sum_{e=1}^{\mathrm{ne}} \left[t_i^{(1)} \int_{(\partial\Omega)_e} N_1 U_{ij}\, \mathrm{d}(\partial\Omega)_e + t_i^{(2)} \int_{(\partial\Omega)_e} N_2 U_{ij}\, \mathrm{d}(\partial\Omega)_e + t_i^{(3)} \int_{(\partial\Omega)_e} N_3 U_{ij}\, \mathrm{d}(\partial\Omega)_e - u_i^{(1)} \times \int_{(\partial\Omega)_e} N_1 T_{ij}\, \mathrm{d}(\partial\Omega)_e - u_i^{(2)} \int_{(\partial\Omega)_e} N_2 T_{ij}\, \mathrm{d}(\partial\Omega)_e - u_i^{(3)} \int_{(\partial\Omega)_e} N_3 T_{ij}\, \mathrm{d}(\partial\Omega)_e \right], \tag{2}$$

where N_i are the shape functions, which are $N_1 = \xi(\xi-1)/2$, $N_2 = (1-\xi)(1+\xi)$, and $N_3 = \xi(\xi+1)/2$; the quantity 'ne' represents the total element numbers on the boundary S; $u_i^{(k)}$ and $t_i^{(k)}$ denote the displacement and traction vectors of the kth node in the element 'e'. By inserting the source point P in each node and performing the integration of Eq. (2), '$2n$' simultaneous equations can be obtained, where 'n' is the total nodes on the discreted boundary S. These are

$$[H]_{2n\times 2n}\{u\}_{2n\times 1} = [G]_{2n\times 2n}\{t\}_{2n\times 1}, \tag{3}$$

where $[H]$ and $[G]$ denote the square matrices containing traction and displacement kernel functions, respectively. In addition, vectors $\{u\}$ and $\{t\}$ represent the collection of nodal displacements and nodal tractions.

2.2. Multi-region boundary element method

Fig. 2 depicts a homogeneous elastic isotropic body containing three kinds of materials. The boundary of material 1 is $S_1 \cup S_4$, and the boundary of material 2 is $S_2 \cup S_4 \cup S_5$. Correspondingly, the boundary of material 3 is $S_3 \cup S_5$.

For the material 1, the systematic equations of BEM are

$$\begin{bmatrix} [H]_{11}^{(1)} & [H]_{12}^{(1)} \\ [H]_{21}^{(1)} & [H]_{22}^{(1)} \end{bmatrix} \begin{Bmatrix} \{u\}_1^{(1)} \\ \{u\}_4^{(1)} \end{Bmatrix} = \begin{bmatrix} [G]_{11}^{(1)} & [G]_{12}^{(1)} \\ [G]_{21}^{(1)} & [G]_{22}^{(1)} \end{bmatrix} \begin{Bmatrix} \{t\}_1^{(1)} \\ \{t\}_4^{(1)} \end{Bmatrix}, \tag{4}$$

where superscript '(1)' denotes material 1. Subscripts '1' in $\{u\}_1^{(1)}$ and $\{t\}_1^{(1)}$ represent the nodal displacements and nodal tractions on boundary S_1 and subscript '4' is for boundary S_4. Moreover, the notations $[H]_{ij}^{(1)}$ and $[G]_{ij}^{(1)}$ denote the submatrices of matrices $[H]$ and $[G]$, respectively.

Similarly, the systematic equations of BEM for materials 2 and 3 can be written as

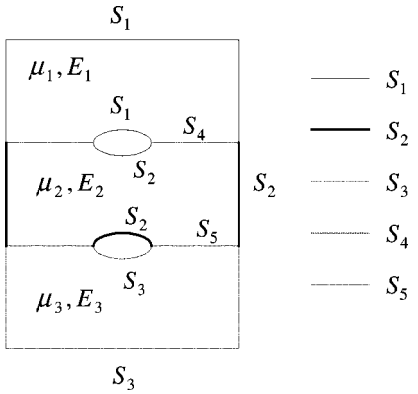

Fig. 2. The boundaries of a three-region BEM.

$$\begin{bmatrix} [H]_{11}^{(2)} & [H]_{12}^{(2)} & [H]_{13}^{(2)} \\ [H]_{21}^{(2)} & [H]_{22}^{(2)} & [H]_{23}^{(2)} \\ [H]_{31}^{(2)} & [H]_{32}^{(2)} & [H]_{33}^{(2)} \end{bmatrix} \begin{Bmatrix} \{u\}_4^{(2)} \\ \{u\}_2^{(2)} \\ \{u\}_5^{(2)} \end{Bmatrix} = \begin{bmatrix} [G]_{11}^{(2)} & [G]_{12}^{(2)} & [G]_{13}^{(2)} \\ [G]_{21}^{(2)} & [G]_{22}^{(2)} & [G]_{23}^{(2)} \\ [G]_{31}^{(2)} & [G]_{32}^{(2)} & [G]_{33}^{(2)} \end{bmatrix} \begin{Bmatrix} \{t\}_4^{(2)} \\ \{t\}_2^{(2)} \\ \{t\}_5^{(2)} \end{Bmatrix}, \tag{5}$$

$$\begin{bmatrix} [H]_{11}^{(3)} & [H]_{12}^{(3)} \\ [H]_{21}^{(3)} & [H]_{22}^{(3)} \end{bmatrix} \begin{Bmatrix} \{u\}_5^{(3)} \\ \{u\}_3^{(3)} \end{Bmatrix} = \begin{bmatrix} [G]_{11}^{(3)} & [G]_{12}^{(3)} \\ [G]_{21}^{(3)} & [G]_{22}^{(3)} \end{bmatrix} \begin{Bmatrix} \{t\}_5^{(3)} \\ \{t\}_3^{(3)} \end{Bmatrix}. \tag{6}$$

Combining Eqs. (4)–(6) allows us to obtain the systematic equations for a three-material composite.

The continuity conditions on the boundary S_4, which are $\{u\}_4^{(1)} = \{u\}_4^{(2)}$ and $\{t\}_4^{(1)} = -\{t\}_4^{(2)}$, and on the boundary S_5, which are $\{u\}_5^{(2)} = \{u\}_5^{(3)}$ and $\{t\}_5^{(2)} = -\{t\}_5^{(3)}$ must be satisfied. In addition, the boundary tractions on the boundaries S_1, S_2, and S_3 prescribed in general and denoted as TT1, TT2, and TT3, respectively, must also be satisfied. Consequently, the continuity conditions as well as the prescribed tractions are substituted into the systematic equations and the unknown quantities on the right hand side of the systematic equations are switched with the known quantities on the left hand side of the systematic equations. In doing so, the systematic equations of the three-region BEM can be expressed in the form as follows:

$$[A]\{X\} = \{B\}, \tag{7}$$

where

$$[A] = \begin{bmatrix} [H]_{11}^{(1)} & [H]_{12}^{(1)} & -[G]_{12}^{(1)} & 0 & 0 & 0 & 0 \\ [H]_{21}^{(1)} & [H]_{22}^{(1)} & -[G]_{22}^{(1)} & 0 & 0 & 0 & 0 \\ 0 & [H]_{11}^{(2)} & [G]_{11}^{(2)} & [H]_{12}^{(2)} & [H]_{13}^{(2)} & -[G]_{13}^{(2)} & 0 \\ 0 & [H]_{21}^{(2)} & [G]_{21}^{(2)} & [H]_{22}^{(2)} & [H]_{23}^{(2)} & -[G]_{23}^{(2)} & 0 \\ 0 & [H]_{31}^{(2)} & [G]_{31}^{(2)} & [H]_{32}^{(2)} & [H]_{33}^{(2)} & -[G]_{33}^{(2)} & 0 \\ 0 & 0 & 0 & 0 & [H]_{11}^{(3)} & [G]_{11}^{(3)} & [H]_{12}^{(3)} \\ 0 & 0 & 0 & 0 & [H]_{21}^{(3)} & [G]_{21}^{(3)} & [H]_{22}^{(3)} \end{bmatrix},$$

$$\{B\} = \begin{bmatrix} [G]_{11}^{(1)} & 0 & 0 & 0 & 0 & 0 & 0 \\ [G]_{21}^{(1)} & 0 & 0 & 0 & 0 & 0 & 0 \\ 0 & 0 & 0 & [G]_{12}^{(2)} & 0 & 0 & 0 \\ 0 & 0 & 0 & [G]_{22}^{(2)} & 0 & 0 & 0 \\ 0 & 0 & 0 & [G]_{32}^{(2)} & 0 & 0 & 0 \\ 0 & 0 & 0 & 0 & 0 & 0 & [G]_{12}^{(3)} \\ 0 & 0 & 0 & 0 & 0 & 0 & [G]_{22}^{(3)} \end{bmatrix} \begin{Bmatrix} \mathrm{TT1} \\ 0 \\ 0 \\ \mathrm{TT2} \\ 0 \\ 0 \\ \mathrm{TT3} \end{Bmatrix}.$$

Eq. (7) can be solved by the method of Gaussian elimination without any difficulty.

3. Stress intensity factor

According to the literature reviewed, the stress behaviors near the crack tips for the four problems in Fig. 1 are not quite the same. Consequently, these four problems in Fig. 1 differ in terms of how to evaluate the SIF or ERR. The following section discusses the formulas of SIF calculation for these associated problems on the basis of the linear elastic fracture mechanics.

3.1. Crack tip located inside the film or inside the substrate

If the crack tip is located within the film or within the substrate (Fig. 1(a) and (d)), the stress has the square root singularity, and hence, the mode-I SIF for the plane strain problem can be evaluated by the form

$$K_{\mathrm{I}} = \frac{E}{4(1-\nu^2)} \lim_{y\to 0^+} \left[\sqrt{\frac{2\pi}{y}}\, u_{xx}(0,y) \right]. \tag{8}$$

A more accurate SIF can be obtained by using the quarter-point element. Therefore, Eq. (8) is rewritten as

$$K_{\mathrm{I}} = \frac{E}{4(1-\nu^2)} \left[\sqrt{\frac{2\pi}{l}}\, (4u_{xx}^{(D)} - u_{xx}^{(E)}) \right], \tag{9}$$

where, quantity l denotes the length of the quarter-point element and superscripts '(D)' and '(E)' represent the nodes 'D' and 'E', as shown in Fig. 3.

3.2. Crack tip terminating at the interface

According to Cook and Erdogan (1972), if the crack tip terminates at the interface (Fig. 1(b)), the stress just ahead the crack tip is

$$\sigma_{xx}(0,y) = b\frac{\sigma(h_{\mathrm{f}})^s}{(-y)^s}, \tag{10}$$

where h_{f} denotes the thickness of the film, b represents dimensionless constant, and s is the stress singularity exponent, which satisfies

$$\cos(s\pi) - 2\frac{\alpha-\beta}{1-\beta}(1-s)^2 + \frac{\alpha-\beta^2}{1-\beta^2} = 0, \tag{11}$$

where α and β are called Dundurs' constants, which are

$$\alpha = \frac{\bar{E}_1 - \bar{E}_2}{\bar{E}_1 + \bar{E}_2}, \qquad \beta = \frac{\mu_1(1-2\nu_2) - \mu_2(1-2\nu_1)}{2\mu_1(1-\nu_2) + 2\mu_2(1-\nu_1)}$$

for the plane strain problem. In the above equation, $\bar{E}_i = E_i/(1-\nu_i^2),\ i = 1,$ and 2 is called material plane strain modulus. The quantities $\mu_i,\ i = 1,$ and 2 represent the shear moduli of material i. Because the power of stress singularity at the crack tip is no longer one-half, the SIF for mode-I crack is defined by

$$K_{\mathrm{I}} = \lim_{y\to 0^-} [(-2\pi y)^s \sigma_{xx}(0,y)]. \tag{12}$$

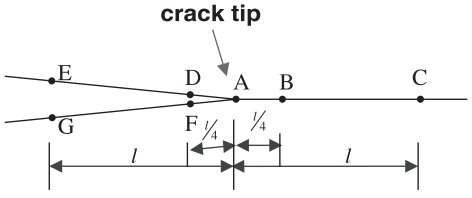

Fig. 3. The quarter-point element near the crack tip.

3.3. Interface crack

Consider a situation in which the crack propagates through the full film and then bifurcates onto the interface of the film and substrate, as shown in Fig. 1(c). The stress and displacement behaviors are the same as those of the interface crack. Hutchinson et al. (1987) observed the asymptotic displacement field near the crack tips of an interface crack. It can be expressed as

$$(u_y + \mathrm{i}u_x)_{\pi} - (u_y + \mathrm{i}u_x)_{-\pi} = \frac{(c_1 + c_2)\mathrm{K}r^{(1/2)+\mathrm{i}\varepsilon}}{(1 + 2\mathrm{i}\varepsilon)2\sqrt{2\pi}\cosh(\pi\varepsilon)}, \tag{13}$$

where the constants $c_1 = (\kappa_1 + 1)/\mu_1$ and $c_2 = (\kappa_2 + 1)/\mu_2$; K denotes the complex intensity factor expressed by $K_1 + \mathrm{i}K_2$ introduced by Sih and Rice (1964); the quantity ε representing the material character is in the form of

$$\varepsilon = \frac{1}{2\pi}\ln\left(\frac{\kappa_1/\mu_1 + 1/\mu_2}{\kappa_2/\mu_2 + 1/\mu_1}\right). \tag{14}$$

In Eq. (14), subscripts 1 and 2 refer to the materials in $y > 0$ and $y < 0$, respectively; the quantity $\kappa = 3 - 4v$ for plane strain and $(3 - 4v)/(1 + v)$ for plane stress.

Taking the real and imaginary parts on both sides of Eq. (13) allows us to set up two simultaneous equations. Then, by solving the simultaneous equations, the real and imaginary parts of the complex-valued SIF, K_1 and K_2, are as follows:

$$\begin{aligned} K_1 &= \frac{D_1}{Q\sqrt{r}}\left(u_y^+ - u_y^-\right) - \frac{D_2}{Q\sqrt{r}}\left(u_x^+ - u_x^-\right), \\ K_2 &= \frac{D_1}{Q\sqrt{r}}\left(u_x^+ - u_x^-\right) + \frac{D_2}{Q\sqrt{r}}\left(u_y^+ - u_y^-\right), \end{aligned} \tag{15}$$

where $Q = (c_1 + c_2)/2\sqrt{2\pi}\cosh(\pi\varepsilon)$, $D_1 = \cos(\varepsilon\ln r) + 2\varepsilon\sin(\varepsilon\ln r)$, $D_2 = \cos(\varepsilon\ln r) - 2\varepsilon\sin(\varepsilon\ln r)$, $u_y^+ = u_y(\pi)$, $u_y^- = u_y(-\pi)$, $u_x^+ = u_x(\pi)$, and $u_x^- = u_x(-\pi)$. The terms of $\cos(\varepsilon\ln r)$ and $\sin(\varepsilon\ln r)$ appearing in Eq. (15), cause a difficulty in numerical calculation when r approaches zero. Therefore, the overall SIF (Tan and Gao, 1990), K_0, representing the maximum amplitudes of these singular stresses, or representing the magnitude of the complex SIF is defined as

$$K_0 = |K| = \sqrt{K_1^2 + K_2^2}. \tag{16}$$

Substituting Eq. (15) into Eq. (16) yields the following expression for the overall SIF:

$$K_0 = \frac{\sqrt{1 + 4\varepsilon^2}}{Q\sqrt{r}}\left[\left(u_x^+ - u_x^-\right)^2 + \left(u_y^+ - u_y^-\right)^2\right]^{1/2}. \tag{17}$$

Eq. (17) indicates that the overall SIF K_0 has square root singularity at the tips of the interface crack.

To calculate the square root singularity, the quarter-point element is applied. According to Blandford (1981), displacements at any point inside the quarter-point element with a distance r from the crack tip can be written as

$$u_i(r) = A_i^{(1)} + A_i^{(2)}\sqrt{\frac{r}{l}} + A_i^{(3)}\left(\frac{r}{l}\right), \tag{18}$$

where l denotes the length of the quarter-point element; $A_i^{(1)} = u_i^{(1)}$, $A_i^{(2)} = (-3u_i^{(1)} + 4u_i^{(2)} - u_i^{(3)})$, $A_i^{(3)} = (2u_i^{(1)} - 4u_i^{(2)} + 2u_i^{(3)})$ and $u_i^{(k)}$ is the displacement vector of the kth node of the quarter-point element.

Substituting Eq. (18) into Eq. (17) yields the expression of the overall SIF in terms of the nodal displacements of the quarter-point elements. Restated,

$$K_0 = \frac{\sqrt{1+4\varepsilon^2}}{Q\sqrt{l}} \left\{ \left[4(u_x^{(D)} - u_x^{(F)}) + (u_x^{(G)} - u_x^{(E)}) \right]^2 + \left[4(u_y^{(D)} - u_y^{(F)}) + (u_y^{(G)} - u_y^{(E)}) \right]^2 \right\}^{1/2}, \tag{19}$$

where superscripts (D), (E), (F), and (G) denote the nodal numbers of the quarter-point elements on the surface of the interface crack, as shown in Fig. 3.

4. Numerical evaluation

For the cracked film–substrate system, the material properties of the film and substrate are both assumed to be linear isotropic and homogeneous. Let Young's modulus and Poisson ratio be denoted as E_1, v_1 for the film and E_2, v_2 for the substrate. Also assumed herein, the cracked film–substrate structure is subjected to a uniform load in the x -direction on the crack surface. Owing to the symmetry with respect to y -axis, only the half space $x \geqslant 0$ is considered.

4.1. Crack tip in the film

First, consider a crack starting from the edge of the film and extending along the direction perpendicular to the interface as shown in Fig. 1(a). The SIF can be evaluated by Eq. (9).

4.1.1. Effects of Dundurs' parameters and crack length on the SIF

To understand how the crack length and Dundurs' parameters influence the SIF, the value of the dimensionless crack length a_f/h_f is taken from zero to one and Dundurs' parameters are chosen as $\beta = 0$ and $\alpha = 0.99,\ 0.8,\ 0,$ and -0.8. Fig. 4 summarizes those results, which correlate very well with those of Beuth (1992) and reveals the following: (i) If the film is stiffer than the substrate (i.e., $\alpha > 0$), the SIF increases with an increasing crack length. More specifically, as the crack tip is near the interface ($a_f/h_f \to 1$), SIF rapidly

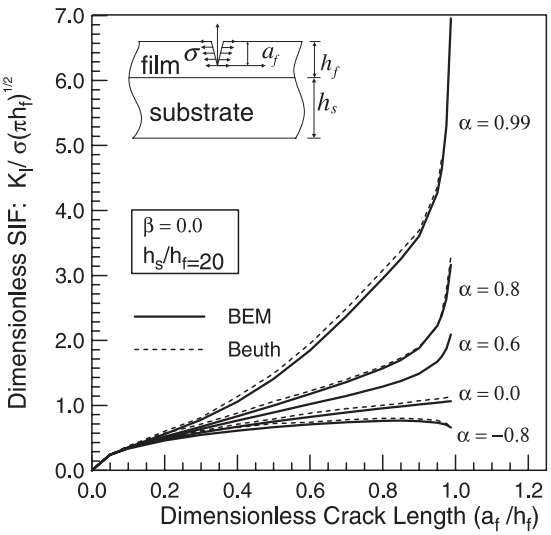

Fig. 4. The effects of the crack length and Dundurs' parameters on SIF of the problem in Fig. 1(a).

increases, which is quite obvious for the case $\alpha = 0.99$; (ii) when the film and substrate have the same elastic properties (i.e., $\alpha = 0$), the normalized SIF $K_I/\sigma\sqrt{\pi h_f} \approx 1$ for $a_f/h_f \to 1$. This phenomenon is attributed to the crack embedded in one material; (iii) For $\alpha < 0$ (the substrate is stiffer than the film), the value of $K_I/\sigma\sqrt{\pi h_f}$ is about 0.8 for $a_f/h_f = 0.2 \sim 0.9$, whereas $K_I/\sigma\sqrt{\pi h_f}$ decreases as the crack tip is nearly terminated at the interface (i.e., $a_f/h_f \to 1$). This observation suggests that if the substrate is stiffer than the film, it is not easy for the cracking to further propagate into the substrate.

4.1.2. Effects of the thickness ratio of the substrate and film on the SIF

Fig. 5 is plotted according to the thickness ratios of the substrate and the film (h_s/h_f) equal to 1, 3, and 10 and the material properties of the film and substrate taken as $\mu_1 = 3\mu_2$, $\nu_1 = \nu_2 = 0.3$. This figure indicates that the thicker the substrate implies a lower amount of SIF. However, the SIF varies only slightly when the ratio h_s/h_f increases from 3 to 10. This finding suggests that if the ratio h_s/h_f is more than 10, the value of SIF is nearly the same as that of $h_s/h_f = 10$.

4.2. Crack tip terminating at the interface

Interestingly, the crack tip is located on the interface of the film and the substrate, as illustrated in Fig. 1(b). As for this problem, the stress behavior at the crack tip has been mentioned in Section 3.2. The SIF can be evaluated by Eq. (12).

4.2.1. Effects of Dundurs' parameters α and β on the SIF

To understand the effects of Dundurs' parameters on SIF, take $\beta = 0$ and $\beta = \alpha/4$, while α is changed form -1 to 1. Fig. 6 plots the relation of the dimensionless SIF, $K_I/\sigma(\pi h_f)^s$, and Dundurs' parameter α. This figure reveals the following: (i) the value of $K_I/\sigma(\pi h_f)^s$ decreases with an increase of the parameter α from -1 to 1 for $\beta = 0$ as well as $\beta = \alpha/4$. This occurrence is attributed to that when α increases, σ does as well, subsequently, decreasing the dimensionless SIF; (ii) For $\alpha < 0$, the value of $K_I/\sigma(\pi h_f)^s$ for $\beta = \alpha/4$ is less than that for $\beta = 0$; while for $\alpha > 0$, the value of $K_I/\sigma(\pi h_f)^s$ for $\beta = \alpha/4$ is larger than that for $\beta = 0$.

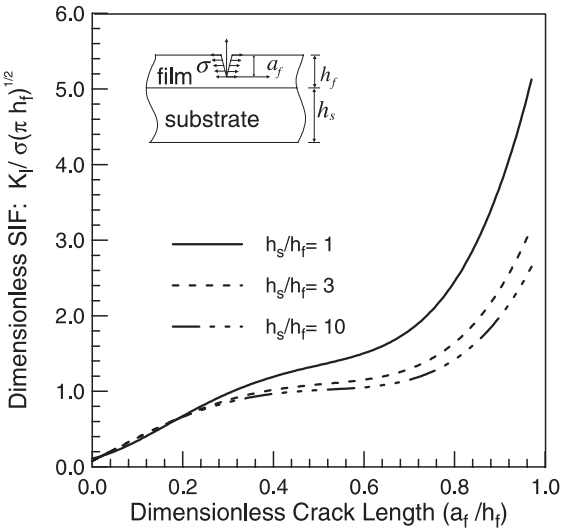

Fig. 5. The effect of the thickness ratio on SIF of the problem in Fig. 1(a).

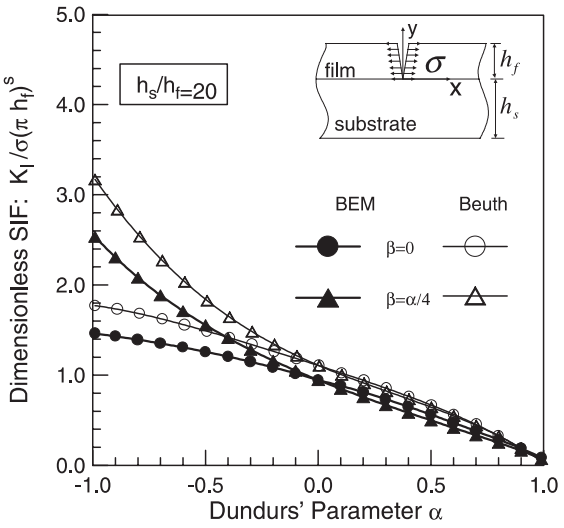

Fig. 6. Dundurs' parameters α versus SIF of the problem in Fig. 1(b) for $\beta = 0$ and $\beta = \alpha/4$.

The results in Fig. 6 slightly differ from those of Beuth (1992). However, when $\alpha = \beta = 0$, in the absence of elastic mismatch, the value of $K_I/\sigma(\pi h_f)^s$ should be equal to 1. According to our results, the value of $K_I/\sigma(\pi h_f)^s$ for $\alpha = \beta = 0$ is 0.95, in which the error is 5%; but in Beuth's result, the value of $K_I/\sigma(\pi h_f)^s$ is 1.11, in which the error is 11%.

4.2.2. Effects of the thickness ratio h_s/h_f on the SIF

Consider the thickness ratios (h_s/h_f), which are chosen as 1, 2, 3, 4, 6, and 20. Figs. 7 and 8 summarize the results for $\beta = 0$ and $\beta = \alpha/4$, respectively. According to these figures, $K_I/\sigma(\pi h_f)^s$ decreases with increasing h_s/h_f. In addition, the difference of $K_I/\sigma(\pi h_f)^s$ between $h_s/h_f = 1$ and $h_s/h_f = 2$ is significantly higher than that of $K_I/\sigma(\pi h_f)^s$ between different thickness ratios. Moreover, if the thickness ratio $h_s/h_f = 1$, the dimensionless SIF, $K_I/\sigma(\pi h_f)^s$, has a maximum value at $\alpha = -0.6$ for $\beta = 0$ and at $\alpha = -0.8$ for $\beta = \alpha/4$.

4.3. Interface crack

When the crack penetrates the film and then propagates along the interface of the film and substrate, as shown in Fig. 1(c), the stress behavior near the crack tip of this problem is the same as that of the interface crack. For the plane strain problem, the ERR for the interface crack problem of Fig. 1(c) denoted as G_i can be calculated by the equation as follows (Suga et al., 1988):

$$G_i = \left[\frac{1-\nu_1}{\mu_1} + \frac{1-\nu_2}{\mu_2}\right] \frac{K\bar{K}}{4\cosh^2(\pi\varepsilon)}, \tag{20}$$

where K denotes the complex-valued SIF and $\bar{K}$ represents the conjugate of K. The quantity $(K\bar{K})^{1/2}$ is the overall SIF, K_0, named by Tan and Gao (1990) and can be evaluated using Eq. (19). Therefore, as long as the overall SIF K_0 is obtained, the ERR G_i of the interface crack can calculated by Eq. (20).

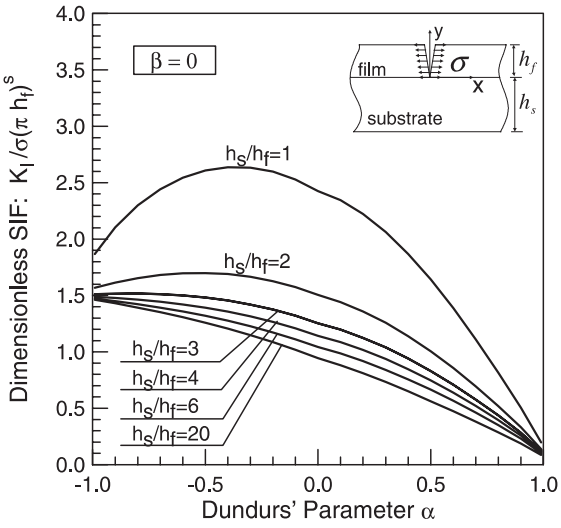

Fig. 7. The effect of the thickness ratio on SIF of the problem in Fig. 1(b) for $\beta = 0$.

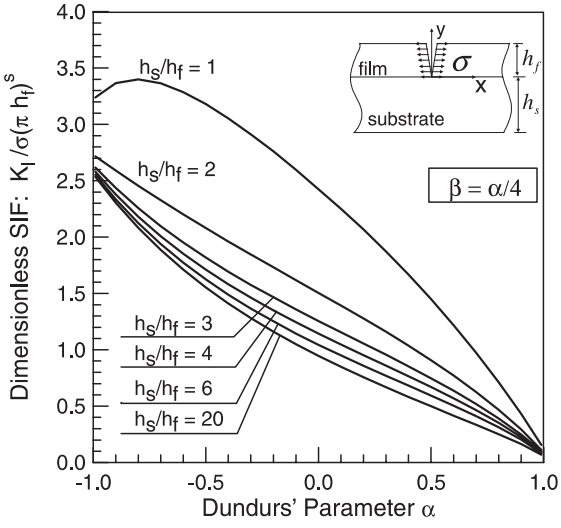

Fig. 8. The effect of the thickness ratio on SIF of the problem in Fig. 1(b) for $\beta = \alpha/4$.

4.3.1. Effects of Dundurs' parameters and the crack length on G

For this interface crack problem, examining the variations of the normalized ERR for various combinations of Dundurs' parameters is a worthwhile task. The following data are used: $\beta = \alpha/4$, $\alpha = 0.6$, 0.2, 0, −0.6, and −0.9; the thickness ratio h_s/h_f is fixed to 20; the ratio of crack length and the film thickness $a_i/h_f = 0^+ \sim 3.0$. Fig. 9 depicts the variations of normalized ERR, $G_i\bar{E}_f/(\sigma^2 h_f)$, versus a_i/h_f according to different parameter α, where $\bar{E}_f = E_1/(1-\nu_1^2)$. It can be seen from Fig. 9 that when the dimensionless crack length $a_i/h_f < 1$, the ERR decreases as $\alpha > 0$; meanwhile, the ERR slowly increases as $\alpha < 0$. Moreover, when $a_i/h_f > 1$, the ERR with the thickness ratio $h_s/h_f = 20$ approaches a constant value for all α. This finding implies that the ERR is in steady state if the crack tip is of a distance of h_f apart from where the load is applied and if the thickness ratio is sufficiently high. Notably, results in this figure slightly differ from

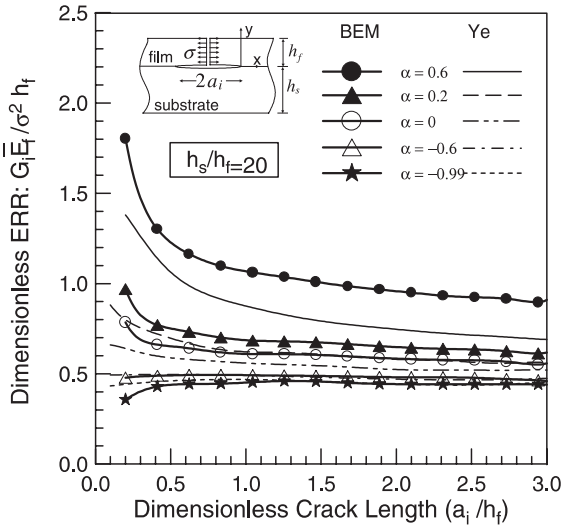

Fig. 9. The effects of the crack length and the parameter α on ERR of the problem in Fig. 1(c) for $\beta = \alpha/4$.

those of Ye et al. (1992). The discrepancies might be because of the inherent inaccuracies induced by the discreteness of the BEM. It is also quite possible that the SIF calculation technique for interface cracks shown in Eq. (19) gives different results from those calculated by the finite element method based on the J-integral.

4.3.2. Effects of the thickness ratio h_s/h_f

The data in Fig. 9 are based on $h_s/h_f = 20$. This section addresses the effect of the substrate thickness on the ERR. For $\alpha = 0.2$ and $\beta = \alpha/4$, Fig. 10 shows the graph of the ERR versus the dimensionless crack length with the variations of $h_s/h_f = 1$, 2, 3, 5, 10, and 20. According to this figure, the thicker the substrate the lower is the ERR value. This figure also reveals that if the substrate thickness is not sufficiently high, e.g. $h_s/h_f = 1$, the ERR has unstable behavior. To investigate this unstable behavior of ERR, let the thickness ratio h_s/h_f be fixed as 1 and Dundurs' parameter α be taken as 0.8, 0.6, 0.2, 0.0, −0.2, −0.6, and −0.8. Fig. 11 summarizes the effects of α on ERR of the interface problem for $h_s/h_f = 1$. According to this figure, although the unstable behavior of the ERR in the problem Fig. 1(c) increases with increasing α, the ERR is stable for a negative α.

4.4. Crack tip located inside the substrate

In this section, we consider the crack propagating into the substrate, as shown in Fig. 1(d). To analyze the problem, the quarter-point element is initially used to calculate the SIF of mode-I crack by using Eq. (9). Then, the ERR G_s of the plane strain problem can be evaluated by

$$G_s = \frac{1 - \nu_2^2}{E_2} K_I^2. \tag{21}$$

Subscript 's' in G_s indicates the ERR for the problem in which the crack tip is located inside the substrate.

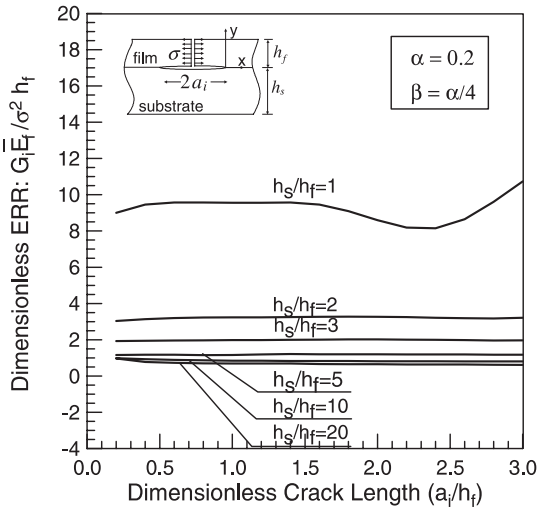

Fig. 10. The effect of the thickness ratio on ERR of the problem in Fig. 1(c) for $\alpha = 0.2$ and $\beta = \alpha/4$.

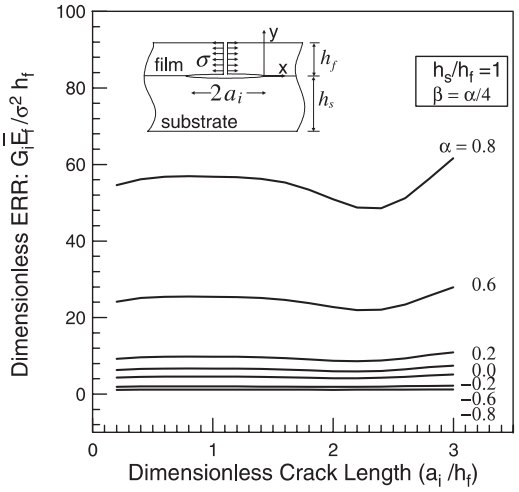

Fig. 11. The effect of the parameter α on ERR of the problem in Fig. 1(c) for $h_s/h_f = 1$.

4.4.1. Effects of crack length and Dundurs' parameters

To study the effects of the crack length and Dundurs' parameters, the dimensionless crack length a_s/h_f is taken from 1^+ to 3.6 and the parameters $\alpha = 0.5$, 0.3, 0, −0.3, and −0.5, $\beta = \alpha/4$ are chosen. The thickness ratio with the thickness ratio h_s/h_f is fixed to 20. Fig. 12 illustrates the variation of the dimensionless ERR, $G_s\bar{E}_f/(\sigma^2 h_f)$, with dimensionless crack length a_s/h_f. According to this figure, the value of G_s increases with increasing α. Moreover, ERR G_s rapidly decreases when the crack tip is near the interface; it also slowly decreases when the crack experiences further growth. However, our results are slightly greater than those of Ye et al. (1992), specially when $a_s/h_f > 3$, the discrepancies are increase. This difference might be attributed

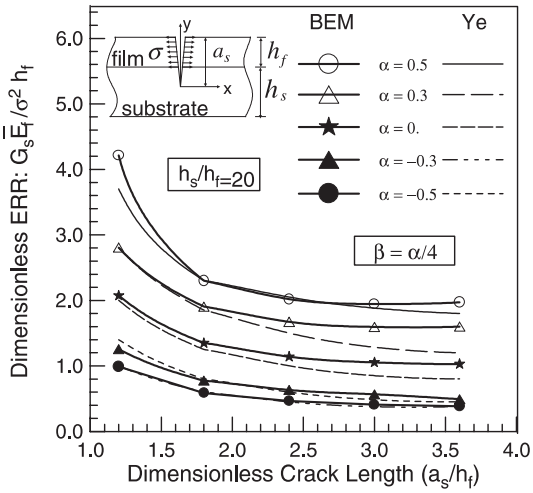

Fig. 12. The effect of the crack length on ERR of the problem in Fig. 1(d) for $h_s/h_f = 20$.

to the effect of the boundary of the substrate on ERR, or the different SIF calculation techniques of interface cracks, as stated in Section 4.3.1.

4.4.2. Effects of the thickness of the substrate

The same problem in Fig. 1(d) is considered herein. However, the thickness ratios (h_s/h_f) equal to 4, 6, 10, and 20 (for fixed h_f) are used. Dundurs' parameters are taken as $\alpha = 0.5$ and $\beta = \alpha/4$. Fig. 13 indicates that if the substrate thickness is sufficiently high, e.g. $h_s/h_f = 20$, ERR is nearly constant for the dimensionless crack length a_s/h_f equal to $1.5 \sim 4.6$. However, when the substrate thickness decreases, i.e., the value of h_s/h_f decreases, and the effects of the boundary of the substrate become obvious. The phenomena associated with the boundary effects can be clearly observed when $h_s/h_f = 4$.

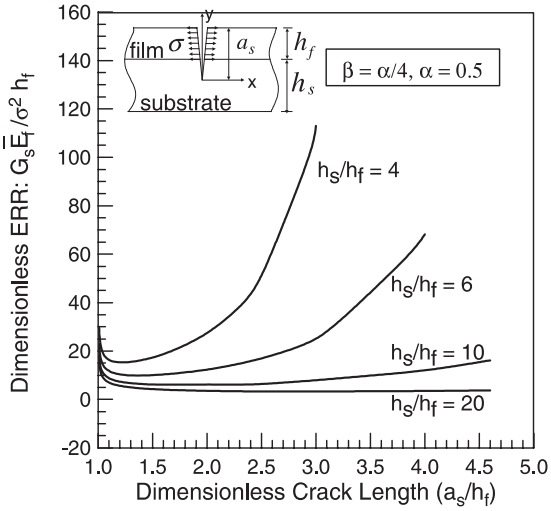

Fig. 13. The effect of the thickness ratio on ERR of the problem in Fig. 1(d) for $\alpha = 0.5$.

5. Conclusions

This study applies the multi-region BEM to analyze the cracked film–substrate material. Based on the results presented herein, we can conclude the following:

(1) *The effects of material mismatch:* If the film is stiffer than the substrate ($\alpha > 0$), the SIF or ERR increases with increasing α; while if the film is weaker than the substrate ($\alpha < 0$), the SIF or the ERR does not markedly change. Moreover, for the problem of Fig. 1(a), when the crack tip approaches the interface ($a_f/h_f \to 1^-$), the SIF or ERR tends to infinity for $\alpha > 0$ but approaches zero for $\alpha < 0$. This observation suggests that the stiffer substrate can protect the crack propagating further, as confirmed by Beuth (1992) and Ye et al. (1992). However, for the problem of the crack tip inside the substrate (Fig. 1(d)), the ERR increases rapidly for all α when the crack tip approaches the interface ($a_s/h_f \to 1^+$);

(2) *The effects of the crack length:* When the crack starts from the edge of the film and propagates normally towards the interface, the SIF increases stably for $a_f/h_f = 0.2 \sim 0.5$. However, SIF rapidly increases for $\alpha > 0$ or decreases for $\alpha > 0$, when the crack is normal and terminated to the interface, as mentioned by Ye et al. (1992). If the crack further extends along the interface, the ERR decreases (for $\alpha > 0$) or increases (for $\alpha < 0$) to a steady-state value. Charalambides et al. (1989) mentioned that the ERR of the interface crack is in steady-state condition if the interface crack length significantly exceeds the film thickness. However, this steady-state behavior is true not only for interface crack length significantly exceeding the film thickness, but also in the condition of a high thickness ratio h_s/h_f; and

(3) *The effects of the thickness ratio:* While the film thickness is fixed and the substrate thickness is changed, the SIF or ERR increases with a decreasing h_s/h_f. Moreover, for the problems of Fig. 1(a) and (b), the variation of the thickness ratio, h_s/h_f, only negligibly influences SIF. However, for the problem Fig. 1(c), if the thickness ratio is small (e.g. $h_s/h_f = 1$), the interface crack becomes quite unstable for a high value of α. In addition, when the crack propagates into the substrate (Fig. 1(d)), the boundary of the substrate greatly influences the ERR.

References

Akisanya, A.R., Fleck, N.A., 1994. The edge cracking and decohesion of thin films. International Journal of Solids and Structures 31, 3175–3199.

Becker, A.A., 1992. The Boundary Element Method in Engineering. McGraw-Hill, New York.

Beuth, J.L., 1992. Cracking of thin bonded films in residual tension. International Journal of Solids and Structures 29, 1657–1675.

Blandford, G.E., 1981. Two-dimensional stress intensity factor computations using the boundary element method. International Journal for Numerical Methods in Engineering 17, 387–404.

Charalambides, P.G., Lund, J., Evans, A.G., McMeeking, R.M., 1989. A test specimen for determining the fracture resistance of bimaterial interfaces. Journal of Applied Mechanics 56, 77–82.

Chen, D.-H., 1984. A crack normal to and terminating at a bi-material interface. Engineering Fracture Mechanics 49, 517–532.

Cook, T.S., Erdogan, F., 1972. Stresses in bonded materials with a crack perpendicular to the interface. International Journal of Engineering Science 10, 677–697.

England, A.H., 1965. A crack between dissimilar media. Journal of Applied Mechanics 32, 400–402.

Erdogan, F., 1988. Stress distribution in a nonhomogeneous elastic plane with crack. Journal of Applied Mechanics 30, Transactions of ASTM, 232–236.

Gecit, M.R., 1979. Fracture of a surface layer bonded to a half space. International Journal of Engineering Science 17, 287–295.

He, M.-Y., Hutchinson, J.W., 1989. Kinking of a crack out of an interface. Journal of Applied Mechanics 56, 270–278.

Hutchinson, J.W., Mear, M., Rice, J.R., 1987. Crack paralleling an interface between dissimilar materials. Journal of Applied Mechanics 54, 828–832.

Kral, E.R., Komvopoulos, K., Bogy, D.B., 1996. Hardness of thin-film media: scratch experiments and finite element simulations. Journal of Tribology 118, 1–11.

Lu, M.-C., Erdogan, F., 1983a. Stress intensity factors in two bonded elastic layers containing cracks perpendicular to and on the interface – I. Analysis. Engineering Fracture Mechanics 18, 491–506.

Lu, M.-C., Erdogan, F., 1983b. Stress intensity factors in two bonded elastic layers containing cracks perpendicular to and on the interface – II. Solution and results. Engineering Fracture Mechanics 18, 509–528.

Matos, P.P.L., McMeeking, R.M., Charalambides, P.G., Drory, M.D., 1989. A method for calculating stress intensities in bimaterial fracture. International Journal of Fracture 40, 235–254.

Rice, J.R., 1988. Elastic fracture mechanics concept for interfacial crack. Journal of Applied Mechanics 55, 98–103.

Sih, G.C., Rice, J.R., 1964. The bending of plates of dissimilar materials with crack. Journal of Applied Mechanics 31, Transactions of ASTM 86, 477–482.

Suga, T., Elssner, E., Schmander, S., 1988. Composite parameters and mechanical compatibility of material joints. Journal of Composite Material 22, 917–934.

Suo, Z., Hutchinson, J.W., 1989. Steady-state cracking in brittle substrates beneath adherent films. International Journal of Solids and Structures 25, 1337–1353.

Tan, C.L., Gao, Y.L., 1990. Treatment of bimaterial interface crack problem using the boundary element method. Engineering Fracture Mechanics 36, 919–932.

Thornton, J.A., 1989. Stress-related effects in thin films. Thin Solid Films 171, 5–31.

Willams, M.L., 1959. The stresses around a fault or crack in dissimilar media. Bulletin of the Seismological Society of America 49, 199–204.

Ye, T., Suo, Z., Evans, A.G., 1992. Thin film cracking and the roles of substrate and interface. International Journal of Solids and Structures 29, 2639–2648.